International Journal of Heat and Mass Transfer 52 (2009) 1284–1294

Contents lists available at ScienceDirect

International Journal of Heat and Mass Transfer

journal homepage: www.elsevier.com/locate/ijhmt

Physical mechanisms of heat transfer during single bubble nucleate boiling of FC-72 under saturation conditions-I. Experimental investigation

Saeed Moghaddam *, Ken Kiger

Department of Mechanical Science and Engineering, University of Illinois at Urbana-Champaign, 1206 West Green Street, Urbana, IL 61801, USA
Department of Mechanical Engineering, University of Maryland, 2181 Glenn L. Martin Hall, College Park, MD 20742, USA

ARTICLE INFO

Article history:
Received 2 April 2008
Received in revised form 22 August 2008
Available online 22 October 2008

Keywords:
Heat transfer
Boiling
Microlayer evaporation
Transient conduction
Microconvection

ABSTRACT

This paper is the first of a two-part study concerning the dynamics of heat transfer during nucleation process of saturated FC-72 liquid. Experimental results discussed in this paper provide new physical insight on the nature of heat transfer events at the nucleation site during the nucleate boiling process. The thermal field underneath a bubble during the boiling of FC-72 was measured with a spatial resolution of 22–40 μm. The time period of activation, area of influence, and magnitude of three different mechanisms of heat transfer active at the nucleation site were determined. These mechanisms consisted of: (1) microlayer evaporation following the rapid bubble expansion, (2) transient conduction due to rewetting of the surface during bubble departure, and (3) microconvection in the region external to the bubble/surface contact area. The area of influence of the transient conduction mechanism was found to be limited to the bubble/surface contact area, with most of the heat transfer occurring prior to the bubble detachment from the surface. The microconvection heat transfer mechanism was localized primarily outside the contact area and was found to be steady in nature. All three mechanisms of heat transfer were found to make significant contributions to the total surface heat transfer. The second part of this study provides the theoretical analysis of the results.

Published by Elsevier Ltd.

1. Introduction

Nucleate boiling represents an important mechanism of heat removal in numerous practical applications ranging from large-scale power plants to small-scale heat sinks. Recent development efforts on some MEMS devices and electronic cooling technologies have placed an emphasis on microphysical processes intrinsic to nucleate boiling. This includes microscale devices that use bubbles for actuation purposes (Lin and Pisano [1], Tsai and Lin [2], and Maxwell et al. [3]), thin-film evaporators (Moghaddam and Ohadi [4]), and spray cooling of electronics (Estes and Mudawar [5], Horacek et al. [6], Shedd and Pautsch [7], Yang et al. [8], and Rini et al. [9]). Studies of Horacek et al. [6], Yang et al. [8], and Rini et al. [9] on spray cooling have clearly indicated formation of numerous bubbles beneath the liquid film sprayed on the heat transfer surface.

Although nucleate boiling has been studied for more than half a century, its physical nature is still plagued with large uncertainties. As can be readily appreciated, a large part of this uncertainty stems from the complex coupling of mass, momentum, and energy transport that occurs between the solid surface, the wetting liquid, and the vapor produced to generate the bubble. The complexity of the problem and the lack of physical understanding of the process have resulted in a plethora of diverse hypotheses concerning the physics of heat transfer processes during boiling. It is common knowledge that bubble generation at the surface is responsible for the observed enhanced heat transfer in boiling. However, details of the heat transfer processes triggered by bubble formation and departure are not clearly understood.

Different and often contradictory hypotheses have been proposed to describe the nature of surface heat transfer during the bubble formation and departure processes. The existing mechanistic boiling heat transfer models can be classified in three different categories: (1) those that have drawn similarities between bubble-induced convective motions near the surface and different single phase convection regimes [10–13] (specifically, forced convection [11], inverted stagnation flow [12], and turbulent natural convection [13]); (2) models suggesting that heat transfer to the liquid takes place via a transient conduction process during the waiting period with bubbles acting as micropumps to remove superheated liquid from the wall as they grow and depart from the surface [14,15]; and (3) composite models that incorporate different mechanisms of heat transfer and often include the latent heat transfer mechanism [16–21].

Although great efforts have been devoted to development of these models, the necessary experimental tools were generally not available at the time to test the basic assumptions upon which

* Corresponding author. Tel.: +1 217 244 5136; fax: +1 217 244 6534.
E-mail address: saeedmog@uiuc.edu (S. Moghaddam).

0017-9310/$ - see front matter Published by Elsevier Ltd.
doi:10.1016/j.ijheatmasstransfer.2008.08.018

Nomenclature

D_b	bubble diameter [m]
D_c	diameter of bubble/surface contact area [m]
f	bubble departure frequency [1/s]
k_{BCB}	thermal conductivity of Benzocyclobutene (BCB) [W/m.K]
q''	heat flux [W/m^2]
Q	heat transfer [J]
R_b	maximum bubble radius [m]
R_c	maximum radius of bubble/surface contact area [m]
t	time [s]
t_b	bubble growth time [s]
t_0	bubble initiation time [s]
T_{H-1}	temperature of H-1 sensor [°C]
T_{H-2}	temperature of H-2 sensor [°C]
T_i	temperature of sensor array [°C]
T_s	surface temperature [°C]

Greek symbols

ΔT	temperature difference between top and bottom of BCB film [°C]
Δx	thickness of BCB film [m]

they are based (i.e., the microphysics of the heat transfer processes active at the nucleation site). The performance of the models has often been evaluated based on their ability to predict the overall surface heat transfer coefficient, which is the cumulative effect of all microscale boiling subprocesses, whether they were incorporated into the model or not. While this bulk measure is the quantity of engineering interest, such a simple validation metric is insufficient to answer why a particular model fails.

The need for understanding the nature of the heat transfer events at the nucleation site has inspired numerous single bubble experimental studies [2,22–35]. In addition to understanding of this fundamental building block of the boiling process, the results are often considered to be scalable to the isolated bubble boiling regime. At higher heat fluxes, however, as conditions progress toward fully developed nucleate boiling conditions, complex bubble-bubble interactions takes place that affects the heat transfer field underneath the bubble. These effects haven't been much studied due to difficulties of conducting experiment in such regimes.

In addition, promising advances have been made during the last decade in the development of multi-scale direct numerical simulation of heat and mass transfer processes involved in nucleation process (i.e. bubble formation and departure). Such works typically integrate microphysical models of the contact region dynamics with a meso-scale formulation to directly simulate the heat and mass transfer during a single bubble ebullition event (e.g., in Lee and Nydahl [36], Son et al. [37], Liao et al. [38], and Genske and Stephan [39]). Contributions from these simulations have been fruitful for exploring the role of the microphysical sub-processes, but most of the simulations are, by necessity, limited to comparisons of bulk quantities with experimental results such as bubble geometry and net heat flux from the surface. Additional experimental work that can quantify the local thermal and fluid variables at a spatial and temporal resolution comparable to the simulations can greatly advance this field.

The advent of new microfabrication materials and methods in recent years has provided an opportunity to conduct such studies. The current work is focused on the task of understanding the microscale physics of processes that control the surface heat transfer underneath a bubble in single bubble boiling process. The study was conducted through use of a novel microelectromechanical (MEM) device that generates single bubbles from an artificial nucleation site and determines the thermal field underneath and around the bubble. Although this study is not intended to directly address complicated boiling processes resulting from multiple bubble interactions on actual boiling surfaces, it paves the way for future studies on such higher order effects.

The details of the design and fabrication process of the device, its unique advantages over the other microscale devices used in prior studies [2,22–35], along with an example test result have been discussed in Moghaddam et al. [40]. Further details can also be found in Moghaddam [41]. This study is focused on using the device to examine different aspects of the heat transfer mechanisms and their variations with surface temperature. The study was conducted with FC-72 liquid at saturation conditions.

2. Test article

The test article consists of a 60-μm thick 3.6 × 3.6 mm^2 square-shape silicon membrane coated with a multi-layer benzocyclobutene (BCB) film with a total thickness of 10.2 μm (cf. Fig. 1). A set of temperature sensors (referred to as H-1 and H-2) within and on the surface of the composite wall (forty-four radially distributed array around three closely spaced cavities, see Figs. 2 and 3) are designed to measure the temperature of the wall surface, both beneath the bubble on the liquid–solid interface, as well as on the interior boundary within the composite solid. This design of the sensor enabled accurate and high resolution calculation of the surface heat flux, since temperature of the top and bottom of the thin BCB layer is known. Also, a preliminary test on a bare silicon membrane indicated that the temperature of the silicon surface remains fairly constant during the nucleation process due to the high thermal conductivity of silicon. More details about the device and its fabrication process are available in Moghaddam et al. [40].

Note that the recent studies [30,33,34] that have used a microheater array on a quartz substrate needed to make some assumptions regarding the heat loss through the substrate in order to determine heat flux at the sensor array area. For example, Myers et al. [34] assumed that the heat transfer regime outside their 1 × 1 mm^2 microheater array (fabricated on a 0.5-mm thick quartz

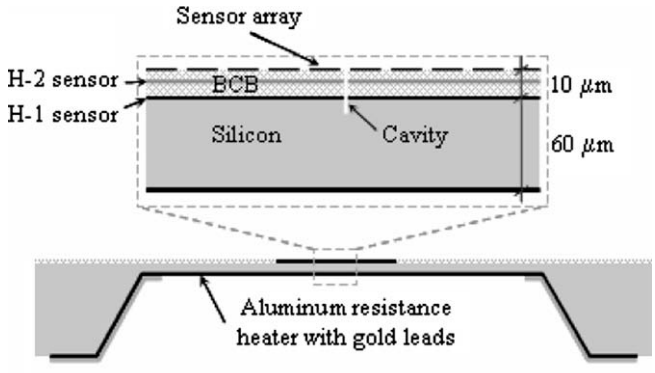

Fig. 1. Schematic cross section of the composite wall with embedded sensors. All temperature sensors are Resistance Temperature Detectors (RTD). Material of the sensors is Ni and their thickness is approximately 10 nm. The H-1 and H-2 sensors are coil-shape with a diameter of 1 mm. Spacing between the H-1 and H-2 sensors is 7.5 μm. The sensor array is 2.5 μm above the H-2 sensor. The sensor array is covered with a 0.2-μm thick BCB layer. Sensor H-2 was fabricated to only check the total heat flux from the sensor array area.

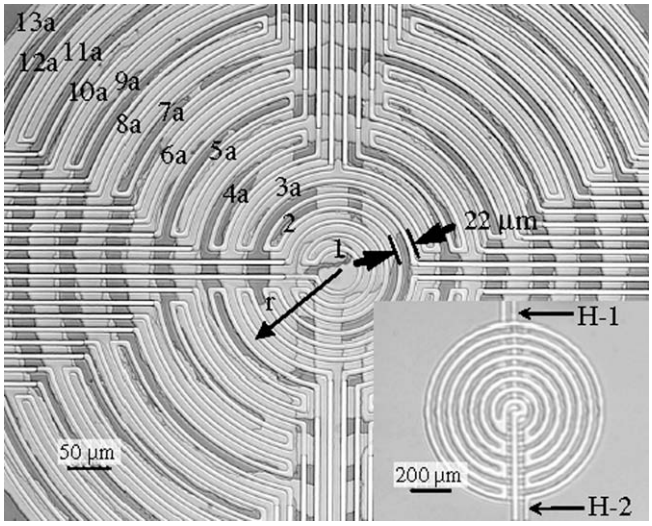

Fig. 2. Close view of device showing sensor array on top of sensors H-1 and H-2. The inset figure shows sensors H-1 and H2 before fabrication of the sensor array.

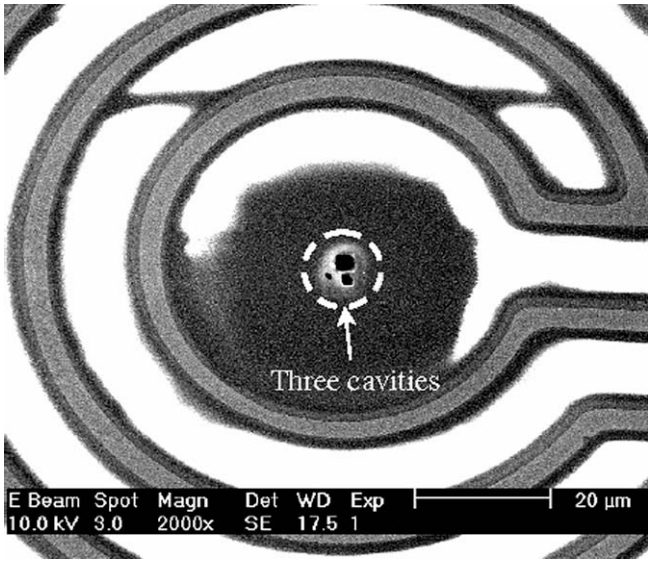

Fig. 3. SEM image of 0.7, 1.3, and 2.4 μm in diameter cavities fabricated using FIB at the center of the sensor array. The three cavities are fabricated on the surface in different sizes to ensure bubble generation over a wide surface temperature range.

substrate) is natural convection with a heat transfer coefficient of 200 W/m^2 K. Using this boundary condition for outside the microheater array area and the experimental temperature data on the microheater array, they numerically calculated the substrate heat loss and surface to fluid heat flux at the array area. The schematic of Fig. 4 illustrates how some of the applied heat by the microheater array dissipates through the substrate. Moghaddam [41] conducted a comprehensive analysis of the substrate heat loss and concluded that different assumptions for thermal boundary conditions outside the array area results in significantly different values for heat flux within the array area. It was shown that the substrate heat loss can be several times greater than the surface to liquid heat flux at the array area.

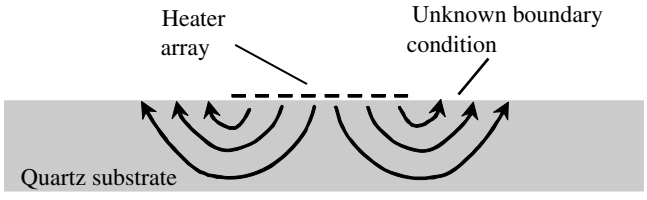

Fig. 4. Schematic cross section of the microheater array on a quartz substrate. Boundary conditions outside the array, temperature distribution within the substrate, and heat loss through the substrate are unknown.

3. Experimental apparatus

The device die is attached to a Pin Grid Array (PGA). The PGA is installed on the bottom cap of the test liquid chamber and is connected from below to a custom-made Signal Conditioning Board (SCB) through a stack of sockets. Fig. 5 shows the liquid chamber and the SCB below it. The output of the SCB is directly connected to an A/D board installed in a PC. The temperature sensors are calibrated with an accuracy of ±0.1 °C. Self-heating of the sensors is negligible (details of the self-heating analysis is available in Moghaddam et al. [40]).

The liquid chamber is connected to a bellows enclosed within a pressure regulated chamber, as can be seen in Fig. 5, in order to adjust the liquid pressure. A hot water line is connected to the external jacket of the liquid chamber to control the test liquid temperature and to provide an isothermal condition. Temperature of the liquid inside the chamber is measured using four thermocouples. The liquid was boiled for several hours to separate non-condensable gas from the liquid. This resulted in repeatable hysteresis events.

A high speed CMOS camera (model Phantom 9, manufactured by Vision Solution, Inc.) monitors the growth and departure of the bubbles from the surface. The camera is synchronized with the A/D board.

4. Data reduction

The surface temperature was controlled by changing the supply voltage to the thin film heater while the temperature of the test liquid was maintained at saturation conditions (56.7 °C at 1 atm). The surface temperature was increased to initiate the boiling (typically the surface temperature was increased to about 130 °C to initially activate the cavity). The boiling onset was associated with generation of many bubbles at the surface and a surface temperature drop. The applied heat to the surface was then gradually reduced to reach the desired surface temperature (defined as the mean temperature of the entire array) with a stable single bubble generated at the artificial cavity. The readings of the temperature sensors were recorded with a frequency of 8 kHz. The camera was configured to acquire bubble images at a framing rate of 8000 frames/s, with an image size of 576 × 576 pixels (resolution is approximately 5 μm/pixel). The images were processed to determine the bubble's equivalent spherical radius (estimated from the bubble outline and assuming axisymmetry) and the apparent contact line (note that the true liquid/vapor/solid contact line is obscured by the bubble). Experimental data were collected at 4 different surface temperatures (T_w = 80.5, 86.4, 91.4 and 97.2 °C, respectively; see Table 1). There was no perceptible waiting time between bubbles in test data Nos. 1–4. As the bubble/surface contact area grew larger with surface temperature, more sensors fell within the contact area and showed a certain temperature variation pattern, which will be discussed shortly. Testing at low surface temperature resulted in two different nucleation regimes; with (test No. 5, T_w = 80.2 °C) and without (test No. 1, T_w = 80.5 °C) waiting time. Detail of the surface temperature variation and its relation with different stages of bubble growth is provided in the following section.

5. Analysis of the temperature results

Fig. 6a shows the images of a bubble at a surface temperature of 80.5 °C (test No. 1). Fig. 6b shows the surface temperature results

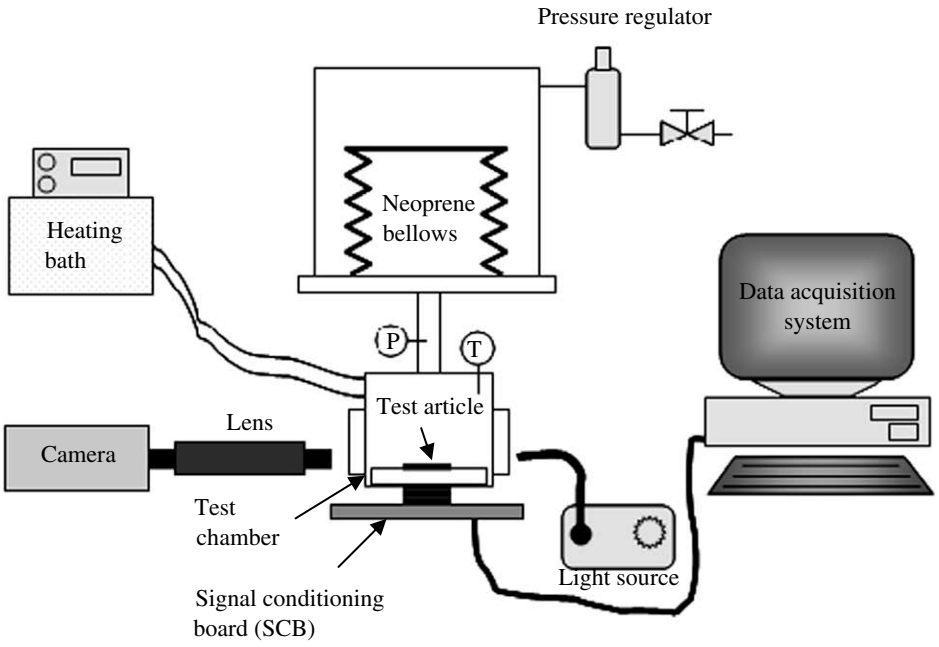

Fig. 5. Diagram of the experimental setup. Test chamber has an external jacket to which hot water is supplied by the heating bath.

Table 1
Experimental results at saturation conditions (56.7 °C at 1 atm)

Test No.	Surface temperature (°C)	D_b [μm]	D_c [μm]	f [1/s]
1	80.5	728	380	125
2	86.4	848	470	112
3	91.4	988	520	92
4	97.2	1110	600	83
5	80.2	798	460	112

corresponding to the bubbling event shown in Fig. 6a. Comparison of the sensor readings within different quadrants of the array at various surface temperatures indicated that the temperature field was axisymmetric (average temperature difference between the four quadrants was typically less than 0.1–0.2 °C). An example of this aspect is provided in Moghaddam et al. [40]). Also, comparison of the temperature results and bubble images for different bubbles suggested that the bubbling events were highly repeatable and quite similar [41].

Comparison of the bubble images (see Fig. 6a) and the temperature data (see Fig. 6b) showed that the initial formation of the bubble at $t_0 = 4$ ms was associated with a sudden drop in surface temperature. The temperature drop started at the center of the array (i.e. at sensor S-1) and progressed over the subsequent sensors (i.e. sensors S-2 to S-4). Comparison of the bubble contact radius with the surface temperature history showed that the temperature drop at each sensor started after the apparent contact line passed over the sensor. The observed temperature drop was due to surface cooling resulting from microlayer evaporation, as suggested in pioneering studies on the subject of microlayer evaporation (e.g. in [22–24,42–45]). The beginning of the microlayer evaporation at each sensor is marked on the temperature profiles shown in Fig. 6b. As can be seen in this figure, the surface temperature started to increase shortly after the initial decline. This indicated that the microlayer was mostly evaporated and the amount of heat supplied to the surface exceeded the cooling due to the microlayer evaporation. The increasing trend in surface temperature continued until the temperature of the H-1 sensor was reached.

A second phase of surface temperature decline started after the bubble/surface contact area reached its maximum diameter and the apparent contact line started to recede. The receding liquid rewetted the dried out area. This rewetting process began at about $t = 8.3$ ms ($t - t_0 = 4.3$ ms). This resulted in a continued decrease in temperature of sensor S-4 that had already significantly decreased due to the microlayer evaporation. The temperature decrease trend passed as a radially inward moving wave, corresponding to when the contact line successively passed over sensors S-3 to S-1.

As can be seen in Fig. 6b, the surface temperature outside the contact area remained unchanged during the entire bubble growth and departure process, with the exception of a small fluctuation in sensor S-5 that is immediately adjacent to the contact area.

As mentioned earlier, test No. 5 (with its significant waiting time between bubble departure and subsequent bubble formation) had a notably different evolution than the other cases. Specifically, the bubble grew rapidly with a nearly hemispherical shape at the beginning of the growth cycle, which was not the case for the bubbles with no waiting time. Fig. 7a shows images of a bubble sequence from test No. 5, $T_w = 80.2$ °C and Fig. 7b shows the corresponding surface temperature field. The bubble cycle was 8.9 ms, which consisted of approximately 6 ms of growth time and a waiting time of 2.9 ms. The highlights of the heat transfer events in this case and their difference with test No. 1 are as follows:

1. The explosive growth of the bubble resulted in a rapid expansion of the contact area over sensors S-1 to 5 in about 1 ms (versus about 3 ms in test No. 1). The cooling rate of the individual sensors was almost twice and the surface experienced a greater temperature drop than in test No. 1, both of which suggest a higher surface heat flux in test No. 5. The microlayer evaporation cooling time (started at $t = 3.84$ ms) was also significantly shorter than in data No. 1. Duration of the cooling time is a function of microlayer thickness, wall temperature, and initial microlayer sensible energy. A thicker microlayer evaporates over a longer period of time, while higher wall temperature and microlayer sensible energy result in faster evaporation.

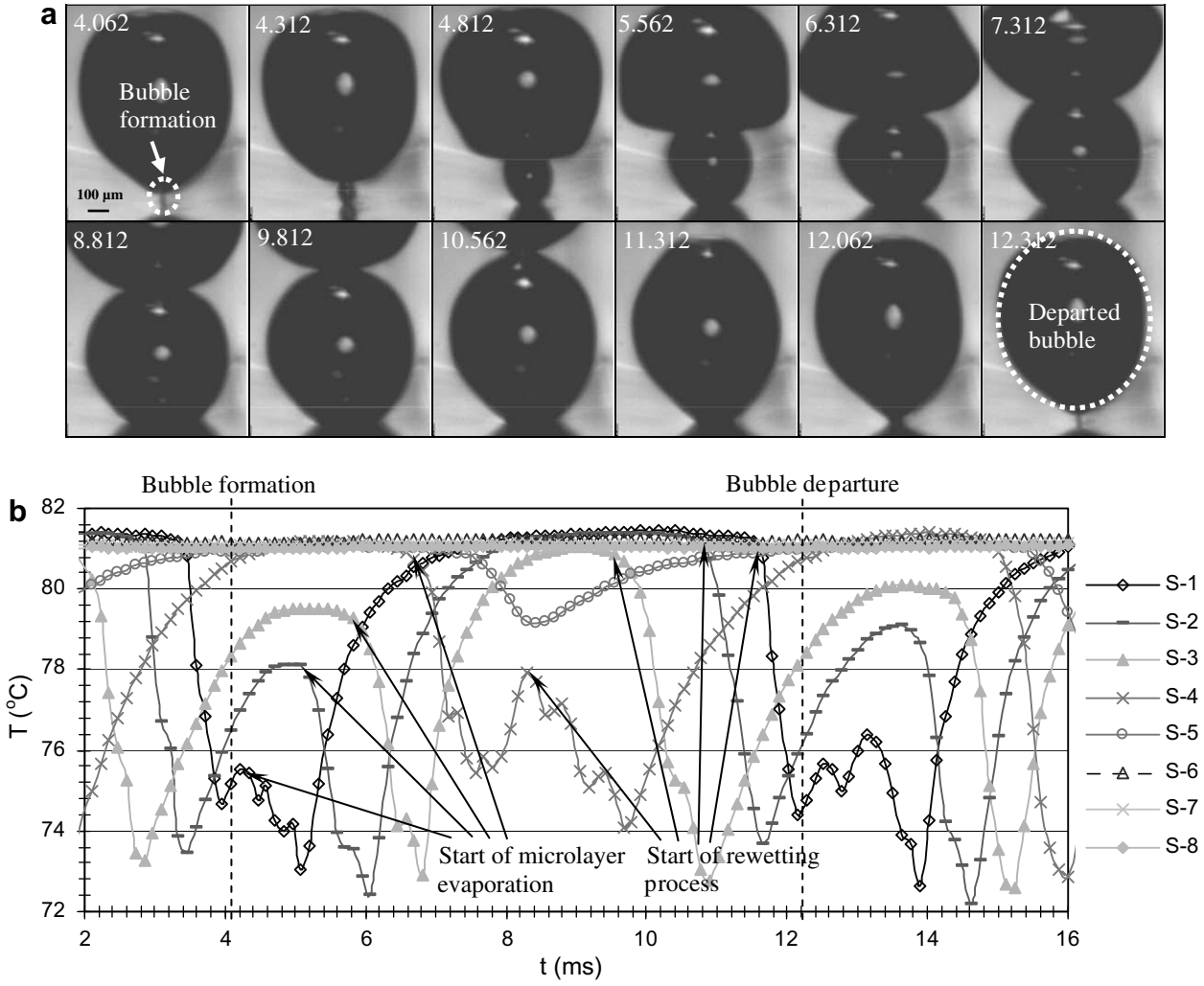

Fig. 6. Test results at surface temperature 80.5 °C (test No. 1 in Table 1). (a) A typical bubbling event. No waiting time exists between the bubbles. Time is in milliseconds. (b) Surface temperature variation during the bubbling event shown in (a).

2. The rewetting time was fairly similar between the two cases (3.5 ms in test No. 5 versus 3.9 ms for test No. 1). However, the waiting time in test No. 5 almost doubled the overall surface cooling duration. In addition, unlike the microlayer cooling events, the amplitude of the surface temperature drop associated with the rewetting process was close between the two tests. This suggested that the surface heat flux during this process was at a similar level in the two cases.

Different aspects of these tests will be further discussed when the heat flux results are presented. The underlying causes of these variations, however, become more clear when the experimental results are theoretically analyzed in part II of this study.

6. Calculation of surface heat flux

To determine the surface heat flux, a numerical model of the BCB layer was built using Icepak (a commercial heat transfer software package developed by Fluent Corporation). Since the temperature results were found to be axisymmetric, modeling only a section of the BCB layer was sufficient to determine the heat flux values, as depicted in Fig. 8. This helped to reduce the mesh count and computational time. The experimental temperature values were applied to their corresponding areas on the model. The other boundary conditions of the model were specified by constant temperature, $T_{H\text{-}1}$, underneath the BCB layer and adiabatic conditions on its three sides.

6.1. Validation

A grid independent solution was determined with a maximum mesh size of 1-, 3- and 2-μm in the *x*, *y*, and *z* coordinate directions, respectively, and a total of 144,791 nodes. At each time step, the solution converged when the normalized energy residuals became less than 10^{-15}. The entire model was initially set at an arbitrary temperature close to the average surface temperature. The results indicated that the influence of the initial conditions on the calculated heat flux diminishes in less than 2 ms. This was verified by changing the solution starting time. Comparison of the numerical heat flux values for a steady state and a transient test case, with uniform temperatures applied to the top and bottom of the model, showed a difference with theory of less than 0.4%.

6.2. Heat flux uncertainty

As mentioned earlier, the temperature was measured with an accuracy of ±0.1 °C. Thermal conductivity of the BCB layer was measured with an uncertainty of ±0.008 W/m K (Moghaddam

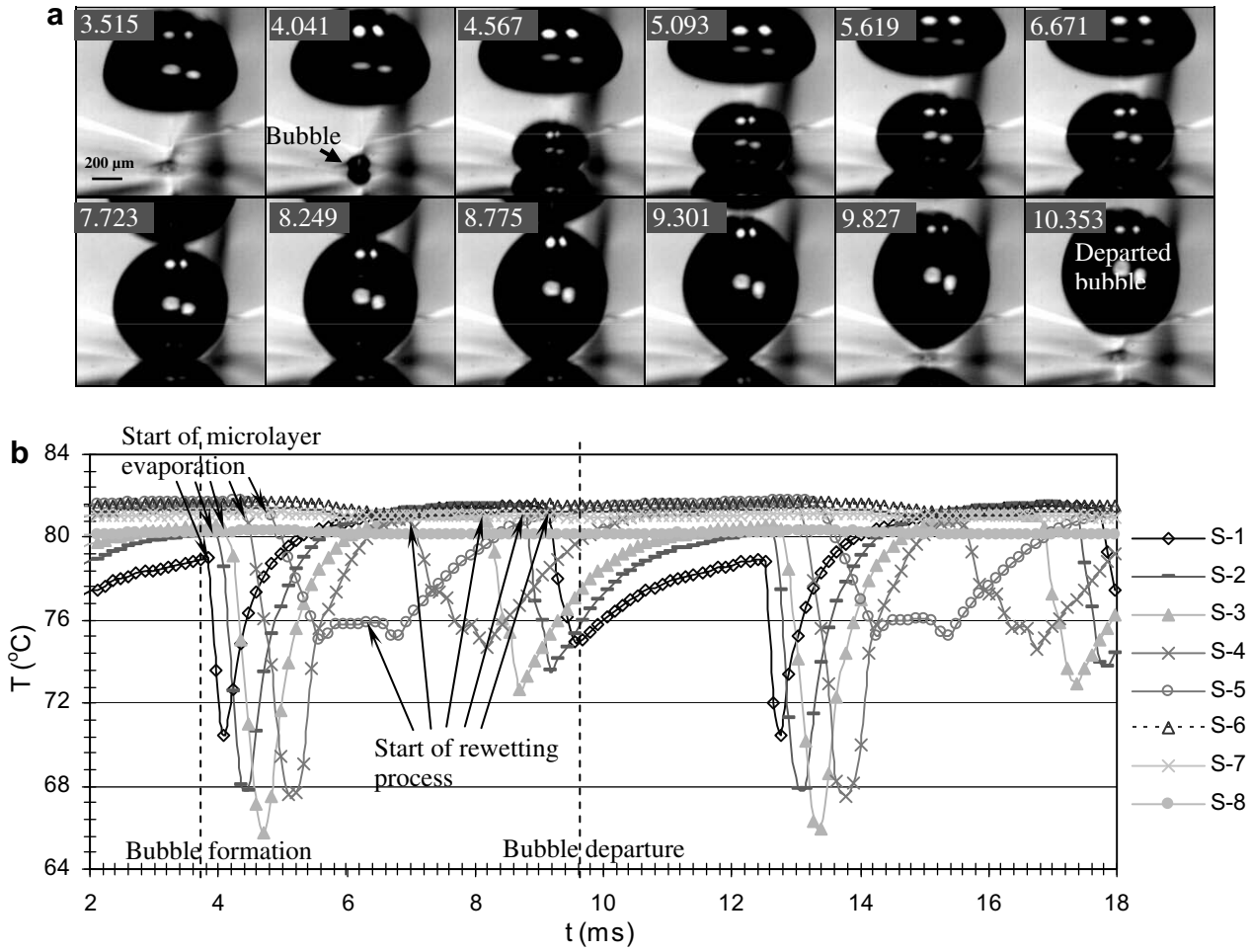

Fig. 7. Test results at surface temperature 80.2 °C (test No. 5 in Table 1). (a) A typical bubbling event. A waiting time of 2.9 ms exists between the bubbles. Time is in milliseconds. (b) Surface temperature variation during the bubbling event shown in (a).

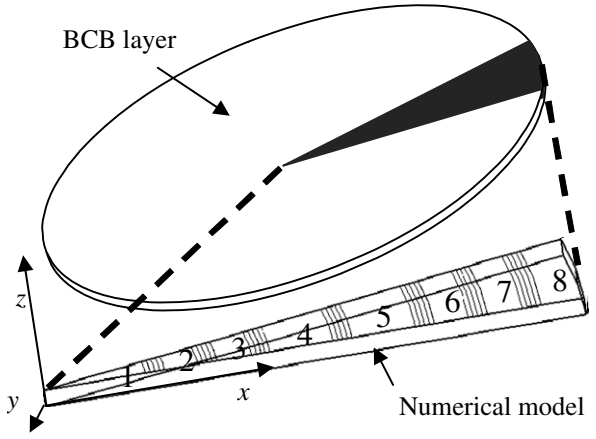

Fig. 8. Numerical model of the BCB layer. Only a section of the BCB layer is modeled due to temperature axisymmetry.

[41]). Also, uncertainty in total thickness of the BCB layer was ±0.2 μm. Contribution of the numerical error to the heat flux uncertainty was considered negligible.

Using all of these uncertainties and the root-mean-square method [46], the heat flux ($q = k_{BCB}\Delta T/\Delta x$) uncertainty was determined to be 4.4% and 7.4% for specific heat flux values of 30 and 3 W/cm^2, respectively. Uncertainty at low heat flux values was dominated by temperature uncertainty. This highlights the critical necessity for precise temperature measurement.

7. Analysis of the heat flux results

The temperature profiles for all test conditions were used in the numerical model of the BCB layer to determine the surface heat flux. The heat flux results for test Nos. 1 and 5 ($T_w \sim 80$ °C, with and without waiting time) are presented in Fig. 9. Interpretation of the heat flux results is provided in the following.

7.1. Microlayer evaporation

As can be seen in Fig. 9a, initiation of the microlayer evaporation process at $t = 4.2$ ms ($t - t_0 \approx 0.2$ ms) resulted in heat flux spikes of up to about 20 W/cm^2 over the contact area. The durations of these spikes were on the order of 1 ms, and correspond to the lifetime of the microlayer over the respective sensor. The peak heat flux value in other test results without waiting time (test Nos. 2–4) increased with surface temperature to about 35 W/cm^2 for the maximum surface temperature of 97.2 °C. The duration of the spikes stayed more or less around 1 ms. As can be seen in Fig. 9b, waiting time in test No. 5 resulted in highest heat flux peaks (in excess of 40 W/cm^2) and a pronounced decrease in microlayer evaporation time.

These data clearly reinforce the results of prior studies [22–24,42–45] regarding the microlayer presence underneath a bubble. The integral over time and area of the heat flux profiles corresponds to the total surface heat transfer due to microlayer evaporation.

7.2. Interline region or micro-region heat transfer

The adhesion force and curvature gradient at the foot of a bubble, where the liquid–vapor interface approaches the wall material, results in a pressure gradient within the liquid that causes liquid flow from the bulk liquid to a wedge shaped thin film region called the interline region [47] or micro-region [48]. Sodtke et al. [35] have recently suggested that a considerable amount of surface heat transfer passes through this region and nucleate boiling heat transfer crucially depends on this mode of heat transfer. They suggested that the typical length of this region is on the order of 1 μm with a heat flux of 100 times greater than in its neighboring liquid. They demonstrated existence of this high heat flux region by generating a large bubble of FC-72 on a downward facing 10 μm thick heated stainless steel foil, brush painted on its backside by a layer of thermochromic liquid crystal (TLC). Temperature of the backside of the wall dropped close to 2 °C (at an applied heat flux of 0.2 W/cm^2) over a 0.6-mm wide region inferring existence of a cooling effect on the opposite side of the wall, at the micro-region.

In order to further investigate the significance of this mode of heat transfer, we used detailed data of Wayner et al. [47]. Wayner et al. [47] determined a length of 0.308 μm and a heat flux of 20 W/cm^2 at the interline region of CCl_4 liquid on a silica surface. If it is assumed that this mechanism is active near the contact line of a bubble with a contact diameter of 500 μm, the heat transfer rate would be 97.2×10^{-6} W. This suggests that heat transfer due to interline evaporation is 0.097 μJ for an arbitrary activation period of 1 ms. This is 2–3 orders of magnitude less than the level of heat transfer we have measured on the sensors. This mode of heat transfer might have contributed to the surface heat flux at the bubble foot for a short time period, but it can not be distinctly seen in our results. However, the net result of this heat transfer event is reflected on the overall surface temperature change and consequently on the heat flux results, since energy is conserved.

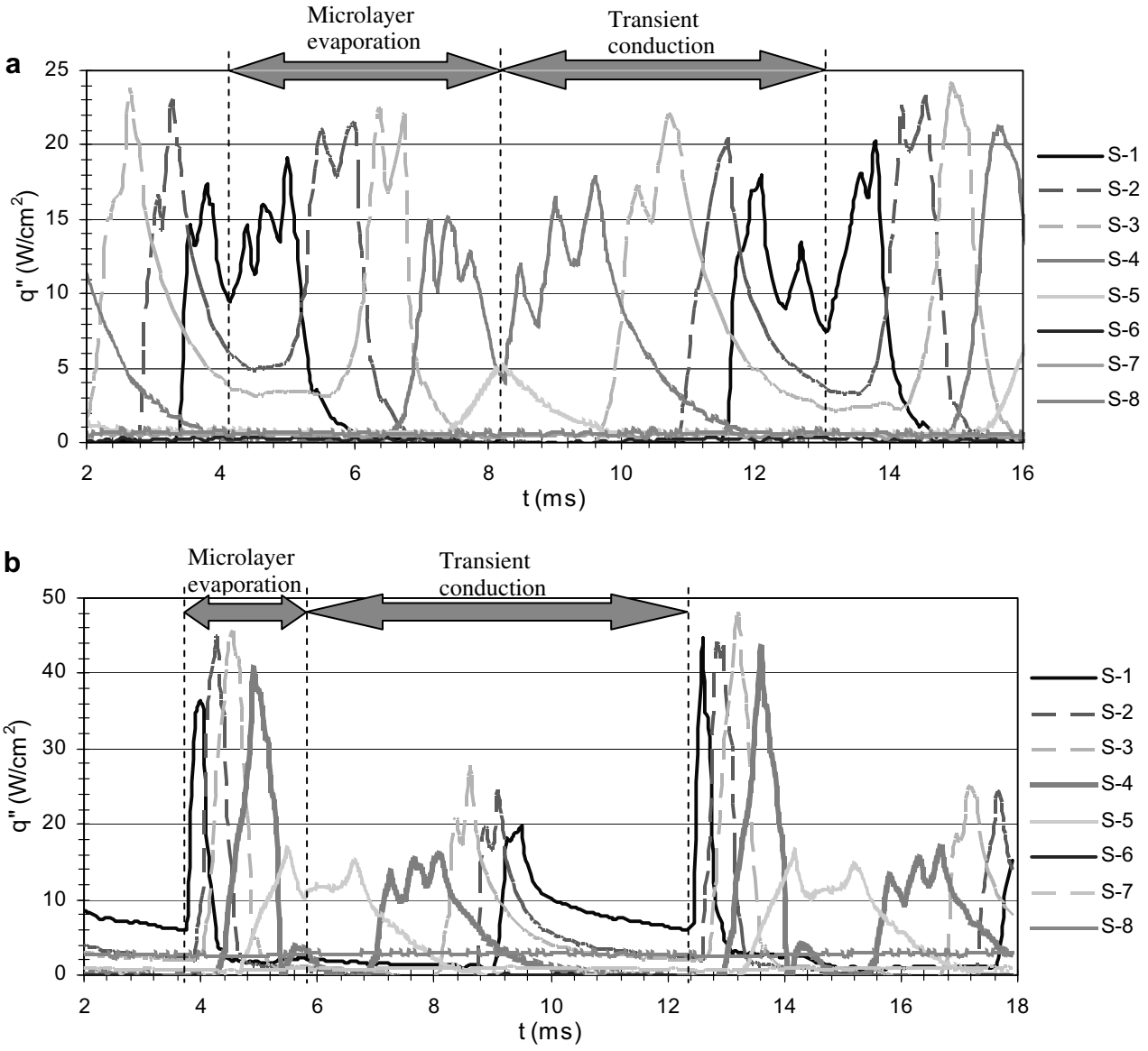

Fig. 9. Heat flux results (a) and (b) corresponding to the temperature data of Fig. 6b and Fig. 7b, respectively. Heat transfer during microlayer evaporation and transient conduction processes are marked.

7.3. Transient conduction and microconvection heat transfer

In addition to the microlayer evaporation discussed above, there are other mechanisms of heat transfer from the surface. The available definitions of these mechanisms in the boiling literature vary widely (as well as the region of the surface over which these mechanisms are presumably active). For example the Mikic and Rohsenow [14] model suggests that a departing bubble pumps away the hot liquid adjacent to the surface from an area twice the bubble diameter. Heat is transferred into the liquid that replaces the displaced fluid via transient conduction, which is considered to be the sole mechanism of heat transfer from the surface. The analogy of Forster and Greif [15] postulates that bubbles act as micropumps in removing the superheated liquid from the surface in a process that was referred to as microconvection. Even the more recent microscale experimental studies [33,34] did not draw a clear distinction between these mechanisms of heat transfer, but rather defined all heat transfer other than the microlayer evaporation as transient conduction/microconvection without determining their relative magnitude and respective spatial localization.

The contribution of the current results, however, allows for a clear distinction between the physics of these two mechanisms of heat transfer, both in terms of their respective magnitude and area of influence. We have considered these mechanisms to be transient conduction and microconvection heat transfer. These two mechanisms are defined in more detail within the following sections.

7.3.1. Transient conduction heat transfer

As mentioned earlier in the discussion of the temperature results, when the contact line starts to recede (e.g. at $t = 8.3$ ms ($t - t_0 = 4.3$ ms) in test No. 1 and $t = 6.1$ ms ($t - t_0 = 2.35$ ms) in tests No. 5), heat flux at the contact area spikes. This mechanism of heat transfer (which primarily takes place inside the contact area) clearly has a transient nature and is consistent with what is commonly named as "transient conduction" mode of heat transfer that results from the rewetting of the superheated wall surface with cooler bulk liquid closer to saturation conditions. The total transient conduction heat transfer from the surface can be determined by multiplying the cumulative heat transfer values by the area of their corresponding sensors and adding them together.

Although the determined heat transfer value represents the transient heat conduction due to surface rewetting by the bubble, it does not entirely represent the transient conduction heat transfer during a bubbling event for tests with no waiting time. This is due to the fact that, even after formation of the subsequent bubble, some areas of the surface are still engaged in the transient conduction heat transfer from the preceding bubble's rewetting process. This can be clearly seen at S-2 and S-3 sensors in Fig. 9a. While a bubble has already formed (and microlayer cooling has peaked at sensor S-1), sensors S-2 and S-3 are still engaged in a decaying transient conduction process until about time 5 ms ($t - t_0 = 1$ ms) and 5.8 ms ($t - t_0 = 1.8$ ms), respectively. A more accurate account of the transient conduction heat transfer during a bubbling cycle can be determined if this factor is also taken into account. Contribution of this portion of transient conduction is about 5% of the total transient conduction heat transfer when no waiting time exists between the bubbles. However, as can be seen in Fig. 9b, during the waiting time of 2.9 ms in test No. 5, the heat transfer on all sensors significantly diminishes, making the transient conduction contribution of the preceding bubble rewetting process negligible.

In addition to the detailed information discussed above, the experimental results revealed several interesting aspects of the transient conduction heat transfer process. The results suggested that the process is active primarily at the bubble/surface contact area (approximately$0.5D_b$). This is in contrast with the Mikic and Rohsenow [14] model that suggested an active area of twice the bubble diameter ($2D_b$), and much closer to the more recent observations of Yaddanapudi and Kim [49]. Mikic and Rohsenow [14] cited Han and Griffith [50] as a basis for their assumption. However, Han and Griffith [50] did not provide a solid reason or any particular experimental evidence for their assumption. They simply assumed that following the departure of a bubble from the heating surface, a piece of superheated liquid from an area twice the bubble diameter is brought into the bulk fluid.

It should also be noted that we do not expect the influence area of this mechanism to be changed by surface thermal properties. For example, in boiling of FC-72 on a thin and low thermal conductivity monolithic substrate, the temperature outside the contact area can change during the transient conduction process. This suggests a different heat transfer dynamic within the substrate not a change in heat transfer regime at the surface/liquid interface within the contact area. The transient conduction mechanism can be simply described as heat transfer during the rewetting of a dried surface that suddenly comes into contact with a cold liquid. If the convection effects within the rewetting liquid layer are assumed negligible, the process resembles the classical transient conduction theory [51] with a small twist that is the surface rewetting is a gradual process, as suggested by Demiry and Kim [33] and Myers et al. [34], rather than being a sudden quenching event. This opinion is reinforced with the good agreement we have found with a modified transient conduction model (presented in part II of this study) that takes into account the gradual coverage of the surface. The transient conduction process is distinctly different from any convection effect that might enhance the surface heat flux immediately outside the contact area.

The test results also indicated that the transient conduction process began after the microlayer evaporation, but before the bubble departure, when the contact line initially started to recede. Results across the different tests suggested that heat flux significantly declines at all sensors prior to formation of the subsequent bubble. For example in Fig. 9a, the only area of the surface that still dissipates a relatively high flux is at sensor S-1. Note that because of its small area the overall contribution of sensor S-1 in total transient conduction heat transfer is relatively small (9.2% in the result shown in Fig. 9a). Therefore, even if formation of another bubble has not immediately followed the departed bubble (i.e. a longer waiting time existed between the bubbles), only a small amount of additional energy would have transferred to the liquid. A clear evidence of such a trend could be seen in test result No. 5. In this test (cf. Fig. 9b), 81.5% of the total transient conduction heat transfer (i.e. 35.2 μJ of a total of 43.2 μJ) occurred before the bubble departure. This is in contrast with the common assumption in the boiling literature (e.g. in [14,30,49]) that the transient conduction process starts after the bubble departure and lasts during the waiting period.

7.3.2. Microconvection heat transfer outside the contact area

As could be seen in the temperature data of Figs. 6b and 7b, the surface temperature outside the contact area remained nearly constant during the cyclic ebullition event in all tests. Considering that the internal silicon/BCB interface temperature ($T_{H\text{-}1}$) was also constant, this implies that the surface heat flux outside the contact area remained constant during the bubble formation and departure process. The value of this heat flux was simply determined using $q'' = k_{BCB}(T_{H-1} - T_s)/\Delta x$. Using the average temperature of the surface outside the contact area as T_s, the corresponding surface heat flux outside the contact area was determined and presented in Fig. 10.

Although the test results suggested that the heat flux outside the contact area was steady during the bubbling event, it was important to determine whether there was any influence of the

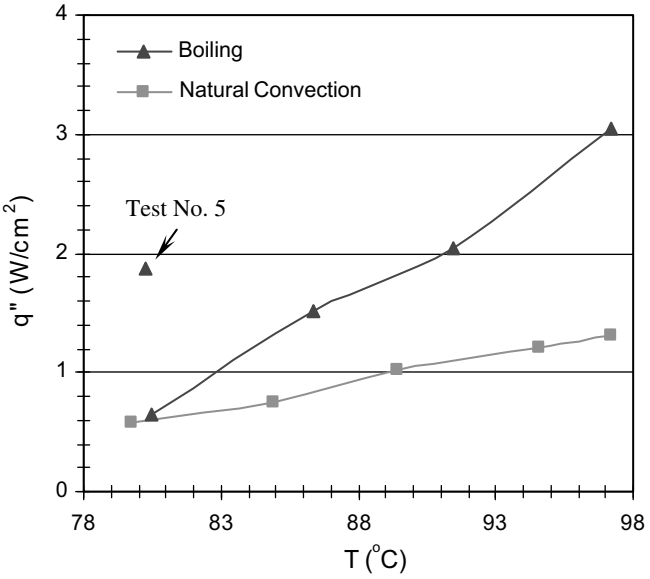

Fig. 10. Comparison of heat flux outside the contact area (i.e. microconvection) with natural convection.

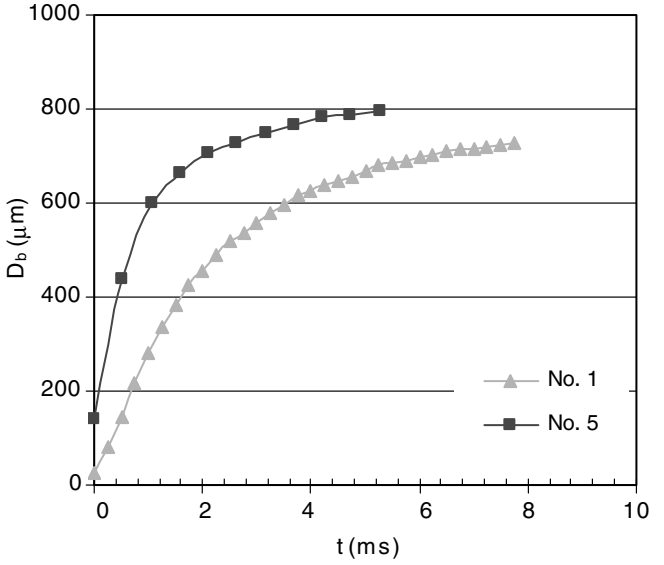

Fig. 11. Difference between bubble growth rate in test Nos 1 and 5. Bubbles grew much faster in test No. 5 than in test No. 1.

bubble on the heat flux outside the contact area or whether the heat flux was simply equal to that of the natural convection, as is frequently assumed in many partitioned boiling models. In order to investigate this important aspect, natural convection heat flux from the surface was measured at the same surface temperature that was used for the boiling test (cf. Fig. 10). This was done by taking advantage of the significant temperature hysteresis (up to about 130 °C) encountered throughout the experiment. Results suggested that bubbling events generated an almost constant enhanced convection effect in the immediate vicinity around the contact area, which can be identified as the microconvection mechanism qualitatively described in previous studies. This process had a steady nature in all test conditions, which is in contrast with some of the exiting models in literature (e.g. in Haider and Webb [16]) that assume a transient nature (i.e. cyclic) for heat transfer outside the contact area.

Comparison of the microconvection and natural convection heat flux at different surface temperatures indicated that the ratio between the two is a strong function of surface temperature. In tests with no waiting time, at low surface temperature, microconvection heat flux was almost the same as the natural convection heat flux. However, the microconvection heat flux significantly surpassed that of the natural convection as the surface temperature was increased. Results indicated that the microconvection heat flux was 2.3 times greater than the natural convection heat flux at a surface temperature of 97 °C.

Microconvection heat transfer in test No. 5 was significantly higher than in test No. 1 even though the surface temperature of both tests was about the same. This difference is certainly due to the difference in growth dynamics of the bubbles between the two cases. The explosive growth (cf. Fig. 11) of the bubble and its faster departure from the surface (cf. Fig. 11) in test No. 5 could have caused the stronger convective effect seen outside the bubble contact area.

8. Variations of the three mechanisms of heat transfer with surface temperature

The heat transfer results (Q) for microlayer and transient conduction mechanisms of heat transfer along with the time period of the bubbling events ($1/f$) were used to determine an average surface heat flux over an area equal to the projected area of the bubble on the surface (πR_b^2). This equivalent average surface heat flux is $q = Qf/\pi R_b^2$. The average of the microconvection heat transfer was also determined by multiplying the measured heat flux value (cf. Fig. 10) by $(R_b^2 - R_c^2)/R_b^2$. Fig. 12a shows the average heat flux values through the three mechanisms. As can be seen in the figure, increase in surface temperature was found to enhance all three mechanisms of heat transfer. While enhancement through the microlayer evaporation and transient conduction mechanisms were found to be moderate, enhancement of the microconvection mechanism was found to be significant. Heat transfer through all mechanisms in test No. 5 was higher than in test No. 1. While heat transfer through transient conduction mechanism was only slightly higher, the enhancement of the two other mechanisms was significant.

The relative contribution of each mechanism to the total surface heat flux was determined by dividing the heat flux through each mechanism by the total surface heat flux (i.e. sum of heat fluxes through the three mechanisms). Fig. 12b shows the relative contribution of each mechanism at different surface temperatures. In tests without waiting time, as the surface temperature was increased from 80 °C to 97 °C, the contributions changed from: (1) 28.8% to 16.3% for microlayer, (2) 45.4% to 32.1% for transient conduction, and (3) 25.8% to 51.6% for microconvection. In test No. 5, the contributions were: (1) 26.5% for microlayer, (2) 32% for transient conduction, and (3) 41.4% for microconvection. Using these results, the following observations about the contributions of the three mechanisms of surface heat transfer were made:

1. Microlayer evaporation was found to make the smallest contribution to the net heat transfer, with its contribution decreasing with increased surface temperature.
2. Transient conduction was found to have the highest contribution among the three mechanisms at low surface temperature, except in test No. 5. However, its contribution fell below that of the microconvection when surface temperature was increased.
3. Microconvection was found to have the least contribution at low surface temperature, except in test No. 5, and the highest contribution at high surface temperature.

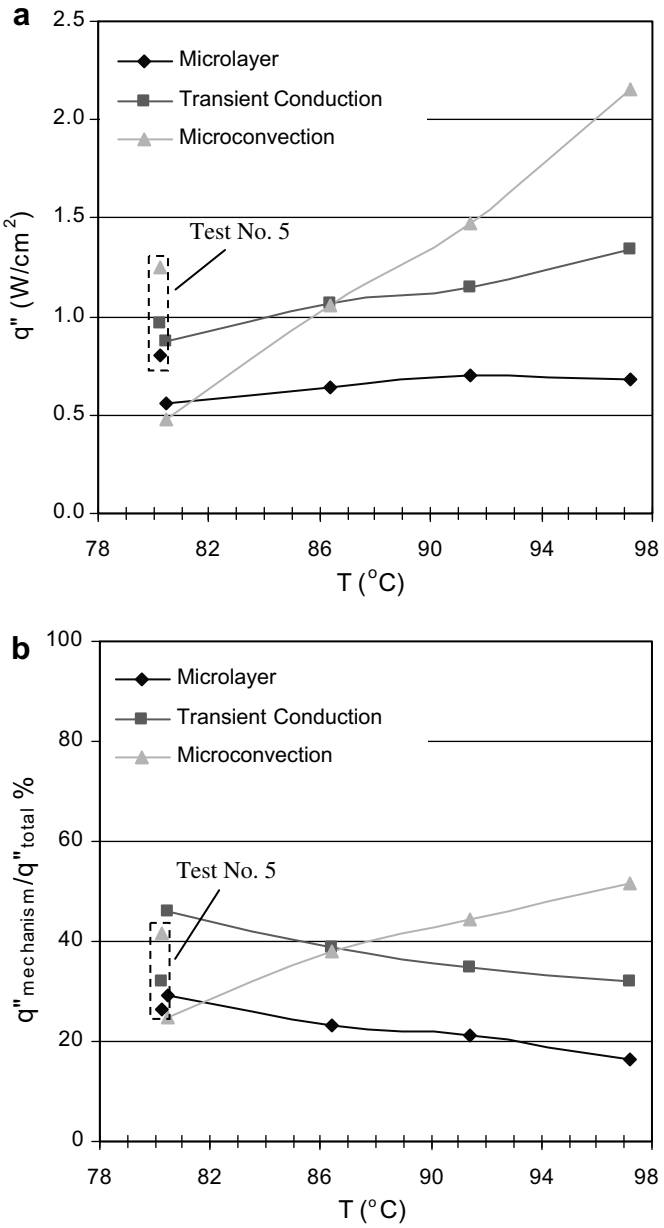

Fig. 12. Variation with surface temperature of (a) surface heat flux through different mechanisms and (b) relative contribution of different mechanisms of heat transfer.

4. The difference in relative contribution of different heat transfer mechanisms in test No. 5 compare to the other tests (i.e. tests without waiting time) was mainly due to the significant enhancement of the microconvection mechanism.

In the part II of this study, the experimental results of this paper will be theoretically analyzed. Simultaneous measurement of all heat transfer events (i.e. magnitude, duration, sequence, and active area) as well as the bubble dynamics parameters (i.e. diameter, departure frequency, and growth and rise velocity) allows us to dissect the models and relate their accuracy to their fundamental assumptions.

9. Conclusions

The thermal field underneath a bubble in boiling of FC-72 liquid was successfully resolved with a spatial resolution of 22–40 μm. The details of the different surface heat transfer mechanisms during the nucleation process including their area of influence, magnitude, and sequence and their relation with different growth stages of the bubble were determined.

The transient conduction heat transfer process was found to predominantly occur at the bubble/surface contact area, and mostly prior to the bubble departure, contrary to what has been commonly assumed in classical boiling models. A clear distinction between this mode of heat transfer and microconvection heat transfer outside the contact area was made. The microconvection heat transfer mechanism was found to have a steady nature. In tests with no waiting time, microconvection heat flux was found to be relatively close to that of the equivalent natural convection heat flux produced by the same geometry and liquid properties, but it was significantly stronger (2.3 times) than natural convection at higher surface temperatures. Also, the explosive growth of the bubbles in a test with waiting time significantly enhanced microconvection (2.9 times greater than natural convection at the same surface temperature).

The exact contribution of the different mechanisms of heat transfer from the surface in single bubble boiling process was directly measured. For a surface temperature range of 80–97 °C under saturation conditions, when no waiting time existed between the bubbles, the contribution of the different mechanisms of heat transfer within a circular area of diameter equal to that of the bubble was found to change from: (1) 28.8% to 16.3% for microlayer, (2) 45.4% to 32.1% for transient conduction, and 3) 25.8% to 51.6% for microconvection. In a test with waiting time, at the lowest surface temperature, the contributions of different mechanisms were: (1) 26.5% for microlayer, (2) 32% for transient conduction, and (3) 41.4% for microconvection.

References

[1] L. Lin, A.P. Pisano, Thermal bubble powered microactuators, Microsyst. Technol. J. 1 (1994) 51–58.
[2] J.H. Tsai, L. Lin, Transient thermal bubble formation on polysilicon microresistors, J. Heat Transfer 124 (2002) 375–382.
[3] R.B. Maxwell, A.L. Gerhardt, M. Toner, M.L. Gray, M.A. Schmidt, A microbubble-powered bioparticle actuator, MEMS 12 (2003) 630–640.
[4] S. Moghaddam, M. Ohadi, Effect of electrode geometry on performance of an EHD thin film evaporator, J. MEMS 14 (2005) 978–986.
[5] K.A. Estes, I. Mudawar, Correlation of Sauter mean diameter and critical heat flux for spray cooling of small surfaces, Int. J. Heat Mass Transfer 38 (1995) 2985–2996.
[6] B. Horacek, K.T. Kiger, J. Kim, Single nozzle spray cooling heat transfer mechanisms, Int. J. Heat Mass Transfer 48 (2005) 1425–1438.
[7] T.A. Shedd, A.G. Pautsch, Spray impingement cooling with single- and multiple-nozzle arrays. Part II: visualization and empirical models, Int. J. Heat Mass Transfer 48 (2005) 3176–3184.
[8] J. Yang, L.C. Chow, M.R. Pais, Nucleate boiling heat transfer in spray cooling, J. Heat Transfer 118 (1996) 668–671.
[9] D.P. Rini, R.-H. Chen, L.C. Chow, Bubble behavior and nucleate boiling heat transfer in saturated FC-72 spray cooling, J. Heat Transfer 124 (2002) 63–72.
[10] M. Jakob, W. Linke, Boiling heat transfer, Phys. Z. 636 (1935) 267–273.
[11] W.M. Rohsenow, A method of correlating heat transfer data for surface boiling of liquids, J. Heat Transfer 74 (1951) 969–976.
[12] C.L. Tien, Hydrodynamic model for nucleate pool boiling, Int. J. Heat Mass Transfer 5 (1962) 533–540.
[13] N. Zuber, Nucleate boiling the region of isolated bubbles and the similarity with natural convection, Int. J. Heat Mass Transfer 6 (1962) 53–78.
[14] B.B. Mikic, W.M. Rohsenow, A new correlation of pool boiling data including the effect of heating surface characteristics, J. Heat Transfer 91 (1969) 245–250.
[15] H.K. Forster, R. Greif, Heat transfer to a boiling liquid-mechanism and correlations, J. Heat Transfer 81 (1959) 43–54.
[16] S.I. Haider, R.L. Webb, A transient micro-convection model of nucleate pool boiling, Int. J. Heat Mass Transfer 40 (1997) 3675–3688.
[17] R.W. Graham, R.C. Hendricks, Assessment of Convection and Evaporation in Nucleate Boiling, NASA TN D-3943, 1967.
[18] R.L. Judd, K.S. Hwang, A comprehensive model for nucleate pool boiling heat transfer including microlayer evaporation, J. Heat Transfer 98 (1976) 623–629.
[19] R.J. Benjamin, A.R. Balakrishnan, Nucleate pooling heat transfer of pure liquids at low to moderate heat fluxes, Int. J. Heat Mass Transfer 39 (1996) 2495–2504.

[20] P. Stephan, J. Hammer, New model for nucleate boiling heat transfer, Heat Mass Transfer/Waerme-und Stoffuebertragung 30 (2) (1995) 119–125.
[21] V.K. Dhir, Boiling heat transfer, Annu. Rev. Fluid Mech. 30 (1998) 365–401.
[22] F.D. Moore, R.B. Mesler, The measurement of rapid surface temperature fluctuation during nucleate boiling of water, AIChE J. 7 (1961) 620–624.
[23] M.G. Cooper, A.J.P. Lloyd, The microlayer in nucleate pool boiling, Int. J. Heat Mass Transfer 12 (1969) 895–913.
[24] R.C. Hendricks, R.R. Sharp, Initiation of Cooling Due to Bubble Growth on a Heating Surface, NASA TN D-2290, 1964.
[25] M.T. Lin, W.J. Yang, L. Lin, A preliminary study of boiling on micro line heaters, Proc. 11th Int. Symp. Transport Phenomena, Hsinchu, Taiwan, 1998.
[26] L. Lin, A.P. Pisano, V.P. Carey, Thermal bubble formation on polysilicon micro resistors, J. Heat Transfer 120 (1998) 735–742.
[27] T. Shimokubo, S. Takagi, T. Inoue, Boiling bubble behavior from the micro heater, Proceedings of 35th Heat Transfer Symposium of Japan, 1998, pp. 173–174.
[28] T.D. Rule, J. Kim, Heat transfer behavior on small horizontal heaters during pool boiling of FC-72, J. Heat Transfer 121 (1999) 386–393.
[29] W.J. Yang, Overview of boiling on microstructures: macro bubbles from micro heaters, Microscale Thermophys. Eng. 4 (2000) 7–24.
[30] F. Demiray, J. Kim, Heat transfer from a single bubble nucleation site during saturated pool boiling of FC-72 using an array of 100 micron heaters, Proceedings of 8th AIAA/ASME Joint Thermophysics and Heat Transfer Conference, St. Louis, Missouri, 2002, pp. 1–12.
[31] H.C. Lee, B.D. Oh, S.W. Bae, M.H. Kim, Single bubble growth in saturated pool boiling on a constant wall temperature surface, Int. J. Multiphase Flow 29 (2003) 1857–1874.
[32] T. Chen, J.N. Chung, An experimental study of miniature-scale pool boiling, J. Heat Transfer 125 (2003) 1074–1086.
[33] F. Demiray, J. Kim, Microscale heat transfer measurements during pool boiling of FC-72: effect of subcooling, Int. J. Heat Mass Transfer 47 (2004) 3257–3268.
[34] J.G. Myers, V.K. Yerramilli, S.W. Hussey, G.F. Yee, J. Kim, Time and space resolved wall temperature and heat flux measurements during nucleate boiling with constant heat flux boundary conditions, Int. J. Heat Mass Transfer 48 (2005) 2429–2442.
[35] C. Sodtke, J. Kern, N. Schweizer, P. Stephan, High resolution measurements of wall temperature distribution underneath a single vapour bubble under low gravity conditions, Int. J. Heat Mass Transfer 49 (2006) 1100–1106.
[36] R.C. Lee, J.E. Nydahl, Numerical calculation of bubble growth in nucleate boiling from inception through departure, J. Heat Transfer 111 (1989) 474–479.
[37] G. Son, V.K. Dhir, N. Ramanujapu, Dynamics and heat transfer associated with a single bubble during nucleate boiling on a horizontal surface, J. Heat Transfer 121 (1999) 623–631.
[38] J. Liao, R. Mei, J.F. Klausner, The influence of the bulk liquid thermal boundary layer on saturated nucleate boiling, Int. J. Heat Fluid Flow 25 (2004) 196–208.
[39] P. Genske, K. Stephan, Numerical simulation of heat transfer during growth of single vapor bubbles in nucleate boiling, Int. J. Therm. Sci. 43 (2006) 299–309.
[40] S. Moghaddam, K. Kiger, A. Modafe, R. Ghodssi, A novel benzocyclobutene-based device for studying the dynamics of heat transfer during the nucleation process, J. MEMS 16 (2007) 1355–1366.
[41] S. Moghaddam, Microscale study of nucleation process in boiling of low-surface-tension liquids, PhD thesis, University of Maryland, College Park, MD, 2006.
[42] T.F. Rogers, R.B. Mesler, An experimental study of surface cooling by bubbles during nucleate boiling of water, AIChE J. 10 (1964) 656–660.
[43] R. Sharp, The Nature of Liquid Film Evaporation During Nucleate Boiling, NASA TN D-1997, 1964.
[44] M.G. Cooper, The microlayer and bubble growth in nucleate pool boiling, Int. J. Heat Mass Transfer 12 (1969) 915–933.
[45] L.D. Koffman, M.S. Plesset, Experimental observation of the microlayer in vapor bubble growth on a heated solid, J. Heat Transfer 105 (1983) 625–632.
[46] L. Ott, Introduction to Statistical Methods and Data Analysis, Duxbury Press, 1977.
[47] P.C. Wayner, Y.K. Kao, L.V. LaCroix, The interline heat transfer coefficient of an evaporating wetting film, Int. J. Heat Mass Transfer 19 (1976) 437–492.
[48] P. Stephan, C.A. Busse, Analysis of the heat transfer coefficient of grooved heat pipe evaporator walls, Int. J. Heat Mass Transfer 35 (1992) 383–391.
[49] N. Yaddanapudi, J. Kim, Single bubble heat transfer in saturated pool boiling of FC-72, Multiphase Sci. Technol. 12 (3–4) (2001) 47–63.
[50] C.Y. Han, P. Griffith, The mechanism of heat transfer in nucleate pool boiling-Part II: the heat flux-temperature difference relation, Int. J. Heat Mass Transfer 8 (1965) 905–914.
[51] H.S. Carslaw, J.C. Jaeger, Conduction of Heat in Solids, second ed., Oxford University Press, London, UK, 1959.